OPEN
Original article

Nuclear Medicine Communications

# Preliminary evaluation of a small interfering RNA molecular probe targeting murine double minute 2 in breast cancer

Xinyu Wang[a,*], Peng Xu[b,*], Yuying Jiao[b], Sha Luan[a], Yue Gao[a], Changjiu Zhao[b,†] and Peng Fu[b]

***Introduction*** **Murine double minute 2 (MDM2) is an oncogene that is important in tumorigenesis, tumor metastasis and chemotherapy resistance. We aimed to synthesize a molecular imaging probe, $^{99m}$Tc-HYNIC-siRNA 1489, which could specifically bind to MDM2. The [$^{99m}$Tc]HYNIC-siRNA 1489 molecular probe provided an effective way of assessing MDM2 expression via single-photon emission computed tomography.**

***Method*** **Three siRNAs were designed, and their inhibitory efficiencies were determined using western blots and qRT-PCR. The selected siRNA was labeled with the radionuclide technetium-99m ($^{99m}$Tc) through the chelator HYNIC. The bioactivity and properties of [$^{99m}$Tc]HYNIC-siRNA 1489 were evaluated prior to imaging in mice. Imaging and biodistribution of the probe were used to assess its targeting ability.**

***Results*** **SiRNA 1489, which was labeled with $^{99m}$Tc, displayed a strong inhibitory effect in Michigan Cancer Foundation-7 cell lines. The radiochemical purity of [$^{99m}$Tc]HYNIC-siRNA 1489 was stable at various temperatures in phosphate-buffered serum and bovine serum. The tumor/muscle ratio in mice injected with [$^{99m}$Tc]HYNIC-siRNA 1489 was higher than that in those injected with the negative control, [$^{99m}$Tc]HYNIC-NC siRNA. The percentage injected dose per gram (%ID/g) of the tumors injected with $^{99m}$Tc-HYNIC-siRNA 1489 was greater than that of the control group.**

***Conclusion*** **The [$^{99m}$Tc]HYNIC-siRNA 1489 was taken up by the tumor, which had a high level of MDM2. The probe exhibited a sufficient retention time in the tumor. This probe may be an effective strategy for evaluating MDM2 expression and achieving early diagnosis in breast cancer. *Nucl Med Commun* 43: 869–876 Copyright © 2022 The Author(s). Published by Wolters Kluwer Health, Inc.**

**Nuclear Medicine Communications** 2022, **43**:869–876

**Keywords: molecular imaging, murine double minute 2, small interfering RNA, technetium-99m**

[a]Department of Nuclear Medicine, The Fourth Affiliated Hospital of Harbin Medical University and [b]Department of Nuclear Medicine, The First Affiliated Hospital of Harbin Medical University, Harbin, China

Correspondence to Peng Fu, PhD, Department of Nuclear Medicine, The First Affiliated Hospital of Harbin Medical University, Harbin 150001, China
Tel: +8613796821565; e-mail: fupeng0451@163.com

*Xinyu Wang and Peng Xu contributed equally to the writing of this article.
†Changjiu Zhao is the co-corresponding author.

**Received** 20 January 2022 **Accepted** 19 April 2022

## Introduction

Breast cancer is the most common tumor in women [1]. It is well known that murine double minute 2 (MDM2), a ubiquitin ligase, can bind p53 and inhibit p53 transactivation of downstream genes [2]. In addition, MDM2 can ubiquitinate p53 and promote its proteasomal degradation [3–5]. As an oncogene, *MDM2* is related to numerous types of human carcinoma, including breast cancer, glioma and prostate cancer [6–8]. MDM2 is able to mediate the Notch pathway by downregulating lysine acetyltransferase 8 (MOF) in breast and liver cancer [9]. MDM2 is an E3 ligase that mediates SIRT6 degradation, and the interaction between MDM2 and SIRT6 is dependent on AKT1-mediated SIRT6 phosphorylation at Ser338 [6,11,12]. Moreover, many studies have shown that MDM2 overexpression is associated with breast cancer that has invasive potential and resistance to chemotherapy [10]. Thus, MDM2 may be considered a promising target for breast carcinoma diagnosis and therapy.

Molecular imaging is a noninvasive method for diagnosing and imaging disease. With the development of molecular imaging technology, many imaging agents have been used in medicine. Small interfering RNA (siRNA), composed of a double strand of RNA, is responsible for RNA interference (RNAi) pathway-based gene silencing. It is incorporated into the RNA-induced silencing complex (RISC) and then Argonaute-2 cleaves the sense strand after siRNA is generated via dicer processing of a long double-stranded RNA or a synthetic siRNA is delivered into the cytoplasm [13]. However, siRNAs have some inherent characteristics, such as off-target effects and biological instability, which need to be addressed before they can be incorporated in clinical applications. Chemical modifications of siRNAs have been shown to improve their inherent properties. For example, representative backbone modifications of siRNA include

phosphorothioate, ribose 2′-OH, and 2′-O-methyl (2′-OMe) modifications. We selected a 2′-OMe modification of the purines based on the following reasons. First, this modification site is the most attractive as it does not need to be recognized by the target mRNA cleavage process via the RISC [14]. Second, 2′-OMe modification increases the resistance of RNA to nucleic acid enzymes, and its thermal stability ($T_m$) increases 0.5–0.7 °C per modification [15]. Third, modification of purine sites does not affect the silencing efficiency of siRNA.

In the present investigation, we used a chemically modified siRNA radiolabeled with technetium-99m ($^{99m}$Tc) to assess MDM2 expression directly via a visual method. The properties of [$^{99m}$Tc]HYNIC-siRNA were assessed in cell experiments. Furthermore, MDM2 imaging was used to assess MDM2 expression in breast cancer xenografts *in vivo*.

## Methods

### Design of the small interfering RNA

Three different siRNAs against MDM2 were designed, and the sequences were as follows: MDM2 475 sense, 5′-GGCCAGUAUAUUAUGACUAd(TT)-3′, antisense, 3′-UAGUCAUAAUAUACUGGCCd(TT)-5′; MDM2 912 sense, 5′-GGAGAUAUGUUGUGAAAGAd(TT)-3′, antisense, 3′-UCUUUCACAACAUAUCUCCd(TT)-5′; MDM2 1489 sense, 5′-CAGCCAUCAACUUC UAGUAd(TT)-3′, antisense, 3′-UACUAGAAGU UGAUGGCUGd(TT)-5′. All siRNAs were modified with 2′-OMe by GenePharma Corp. (Shanghai, China). A primary amine was added at the 5′ end of the antisense RNA. The amine provided a coupling site for HYNIC, which is important for radionuclide labeling. Quantitative real-time PCR (qRT-PCR) and western blots were used to select the optimal siRNA to inhibit MDM2.

### The small interfering RNA radiolabeling and characteristics

The siRNA (5 μg/μl) was diluted in 25 mmol/l ammonium acid carbonate buffer (pH = 8.5). HYNIC (GL Biochem., Shanghai, China) was dissolved in dimethylformamide (10 mg/ml). Then, siRNA was added in the proportion 20:1 (HYNIC:siRNA). The compounds were reacted for 1 h at room temperature. The mixture was purified with a Sep-Pak C18 column (Waters, Milford, Massachusetts, USA). The C18 column was activated by 20 ml of acetonitrile and washed with 20 ml of deionized water. The siRNA and HYNIC mixture was diluted to 1 ml with deionized water and then loaded on the Sep-Pak C18 column, which was rinsed once with 10-ml 25-mmol/l ammonium bicarbonate (pH = 8.5), once with 10-ml 25-mmol/l ammonium bicarbonate/5% acetonitrile, and twice with 10 ml 5% acetonitrile, and then, siRNA was eluted with 1-ml 30% acetonitrile four times. The HYNIC-siRNA solution was collected in fractions of eight drops/vial, HYNIC-siRNA was detected at 260 nm, and vials with the highest concentrations of HYNIC-siRNA were combined. The product was then dried by rotary evaporation for 6 h, and the HYNIC-siRNA was stored at −80 °C.

The HYNIC-siRNA solution was prepared, and tricine and ethylenediamine-N,N'-diacetic acid (EDDA) were used as coligands. Ten microgram of HYNIC-siRNA were dissolved in 20 μl 25 mmol/l ammonium acid carbonate (pH = 8.5). Tricine (50 μl, 5.6 mmol/l) and EDDA (50 μl, 5.6 mmol/l) were added to the HYNIC-siRNA solution. Then, 10–20 μl $^{99m}TcO_4^-$ solution (74–185 MBq; China Isotope & Radiation Corporation, Beijing, China) was diluted with 5.5 μl of $SnCl_2{\cdot}2H_2O$ (4.4 mmol/l in 0.1 mol/l HCl) and mixed with the HYNIC-siRNA solution. After 1 h, the mixture was purified using a G25 gel (Solarbio, Beijing, China). The G25 gel column was eluted with 0.9% NaCl solution, and the eluent was collected (40 tubes with three drops in each tube). The combined eluent with a radioactive peak was used for imaging evaluation and calculating radiochemical purity. [$^{99m}$Tc]HYNIC-siRNA was diluted in PBS and BSA (0.01 μg/μl) and then incubated at room temperature and 37 °C for 6 h. Its stability *in vitro* was evaluated by its radiochemical purity, which was measured by high-performance liquid chromatography at different times. Briefly, the C18 column was eluted with a gradient of 59–100% buffer A (A, 0.1% trifluoroacetic acid in acetonitrile) and 0–40% buffer B (B, 0.1% trifluoroacetic acid in water) in 20 min and a flow rate of 1 ml/min at 30 °C.

### Cell lines and cell culture

Human breast cancer cell lines Michigan Cancer Foundation (MCF)-7 and MDA-MB-231 were purchased from the Chinese Academy of Sciences Shanghai Cell Bank. The cells were cultured in Roswell Park Memorial Institute (RPMI) 1640 complete medium (Gibco, Carlsbad, California, USA) at 37 °C in an incubator containing 5% $CO_2$. The complete medium comprised 10% fetal bovine serum (FBS), penicillin (100 U/ml) and streptomycin (100 μg/ml).

### Transfection of [$^{99m}$Tc]HYNIC-siRNA

MCF-7 cells were trypsinized and transferred to six-well plates at a concentration of $1 \times 10^6$ cells/well. The RPMI 1640 medium was then added to each well. After the cells reached 70% confluency, the medium was replaced with opti-MEM (Gibco, Carlsbad, California, USA). Two micrograms of siRNA 1489, control siRNA, and [$^{99m}$Tc]HYNIC-siRNA 1489 was dissolved in 200 μl opti-MEM, respectively. Eight microliters of Lipofectamine 2000 (Invitrogen, Carlsbad, California, USA) solution were added to each of three 200-μl aliquots of opti-MEM. Then, the Lipofectamine 2000/opti-MEM mixture was added to the siRNA1489, control siRNA, and [$^{99m}$Tc]HYNIC-siRNA 1489 mixtures, which were incubated at room temperature for

20 min. In the final solutions, the siRNA concentration reached 0.01 μg/μl. Then, the liposome-encapsulated control siRNA, liposome-encapsulated siRNA 1489 and liposome-encapsulated [$^{99m}$Tc]HYNIC-siRNA 1489 were individually added to MCF-7 cells and cultured in an incubator (37 °C and 5% $CO_2$) for 6 h. The opti-MEM was removed and complete medium was added. After 24 h, the MCF-7 cells were collected and used for qRT-PCR and western blotting.

### Quantitative real-time PCR

Total RNA was extracted using an RNAprep Pure Cell/Bacteria Kit (Tiangen, Beijing, China) according to the manufacturer's protocol. cDNAs were synthesized from total RNA (1 μg) using random primers with the RevertAid First Strand cDNA Synthesis Kit (Thermo Fisher Scientific, Waltham, Massachusetts, USA). qRT-PCR was performed with the MDM2 and internal reference GAPDH primer set (MDM2 forward, 5′-CCTTAGCTGACTATTGGAAATGCA-3, reverse, 5′-CGAAGGGCCCAACATCTGT-3′; GAPDH forward, 5′-CACCCACTCCTCCACCTTTGA-3′, reverse, 5′-ACCACCCTGTTGCTGTAGCCA-3′) under the following PCR conditions: predenaturation at 95 °C for 60 s, denaturation at 95 °C for 15 s and extension at 60 °C for 60 s, for 40 cycles.

### Western blots

MCF-7 cells were lysed in RIPA buffer with phenylmethylsulfonyl fluoride (100:1) for 30 min on ice and then centrifuged at 12 000 × *g* at 4 °C for 15 min. The supernatant was collected and mixed with SDS-PAGE buffer, denatured, and the total protein was measured using a BCA Protein Assay Kit (Tiangen, Beijing, China). Equal amounts of protein were separated by 10% SDS-polyacrylamide gels and transferred onto polyvinylidene difluoride membranes (Millipore, Billerica, Massachusetts, USA). The membranes were blocked using 5% nonfat milk in TBST for 1 h at 37 °C, followed by overnight incubation with anti-MDM2 (ab178938; Abcam, Cambrige, UK) and anti-β-actin (20536-1-AP; Proteintech, Wuhan, China) antibodies at 4 °C. Unbound antibody was removed by three 10-min washes in TBST solution. The membranes were THEN incubated for 1 h at room temperature with secondary antibody (ZB-2301; Zhong Shan Gold Bridge, Beijing, China) conjugated with horseradish peroxidase, followed by three 10-min washes with TBST buffer (TBS buffer with 0.1% v/v Tween-20). The blots were visualized with enhanced chemiluminescence reagent (Advansta, Menlo Park, California, USA) and a Tanon-5200 Chemiluminescent Imaging System (Tanon Science & Technology, Shanghai, China).

### Animal models

Female NU/NU nude mice (aged 6–8 weeks, body weight 18–22 g) were purchased from Peking Vital River Experimental Animal Co., Ltd (Beijing, China). All protocols involving animals were performed under the supervision of the Institutional Animal Care and Use Committee of Harbin Medical University. The mice were randomly divided into two groups. An MCF-7 cell suspension ($5 \times 10^6$ cells) was directly injected into the right hind limb of each mouse. The mice were maintained in a standard environment with sufficient food and drinking water. The imaging experiments were carried out when the tumor reached 500 $mm^3$ [tumor volume $(mm)^3$ = length (mm) × width $(mm)^2 \times 0.5$].

### Molecular imaging and biodistribution assay

TurboFect (Invitrogen, Carlsbad, California, USA)-encapsulated [$^{99m}$Tc]HYNIC-siRNA 1489 (7.4 MBq) and [$^{99m}$Tc]HYNIC-control siRNA (7.4 MBq) were separately injected into the two groups of mice ($n$ = 6) via the tail vein. Single-photon emission computed tomography (SPECT, Discovery 670; GE Healthcare, Boston, Massachusetts, USA) with a low-energy, high-resolution and pinhole collimator was prepared. At 1, 4, and 10 h after injection, all mice were scanned using SPECT. All mice were subjected to abdominal anesthesia with 1% pentobarbital sodium (0.04 ml/10 g). The static image was set at 100 counts through the pinhole collimator, and then, image acquisition was stopped and the images saved. The matrix was 256 × 256 and the zoom factor was 2.0. The regions of interest of each tumor were drawn and counted. Radiocounting of equal areas of muscle on the opposite limb was recorded as a control. Finally, the tumor-to-muscle (T/M) ratio was calculated.

Thirty-six NU/NU nude mice with MCF-7 xenografts were randomly divided into two groups of 18. A biodistribution study was performed after tail vein injection of TurboFect-encapsulated [$^{99m}$Tc]HYNIC-siRNA3 (7.4 MBq) or [$^{99m}$Tc]HYNIC-control siRNA (7.4 MBq). At 1, 4, and 6 h postinjection, four mice from each group were sacrificed by inhalation of isoflurane followed by cervical dislocation. Major internal organs, including the brain, lungs, liver, spleen, kidneys, stomach, intestines, muscle, thyroid and blood, together with the tumor, were collected and weighed, and the radioactivity was measured via a gamma counter. Tissue radioactivity was represented by the percentage of injected dose per gram (%ID/g) of organ. The mass ratio of the tumor to the contralateral muscle (T/M) was also calculated.

### Blocking assay

Six NU/NU nude mice with MCF-7 xenografts were used in the blocking assay. Nonlabeled siRNA 1489 (1 mg/kg) encapsulated with TurboFect was injected into MCF-7 xenografts 3 h before the injected imaging agent. The imaging procedure was repeated, and tissue radioactivity was represented by the %ID/g.

### Statistical analysis

Each experiment was performed in triplicate with duplicate samples tested. Statistical analysis was performed with SPSS 18.0. Data are expressed as the mean ± SD. Statistical differences were analyzed via one-way analysis of variance. $P < 0.05$ was considered statistically significant.

## Results

### Expression of murine double minute 2 in breast cancer cell lines

To select suitable cell lines with high levels of MDM2, qRT-PCR and western blots were used to evaluate MDM2 expression in MCF-7 and MDA-MB-231 cells. The results showed that the relative expression levels

**Fig. 1**

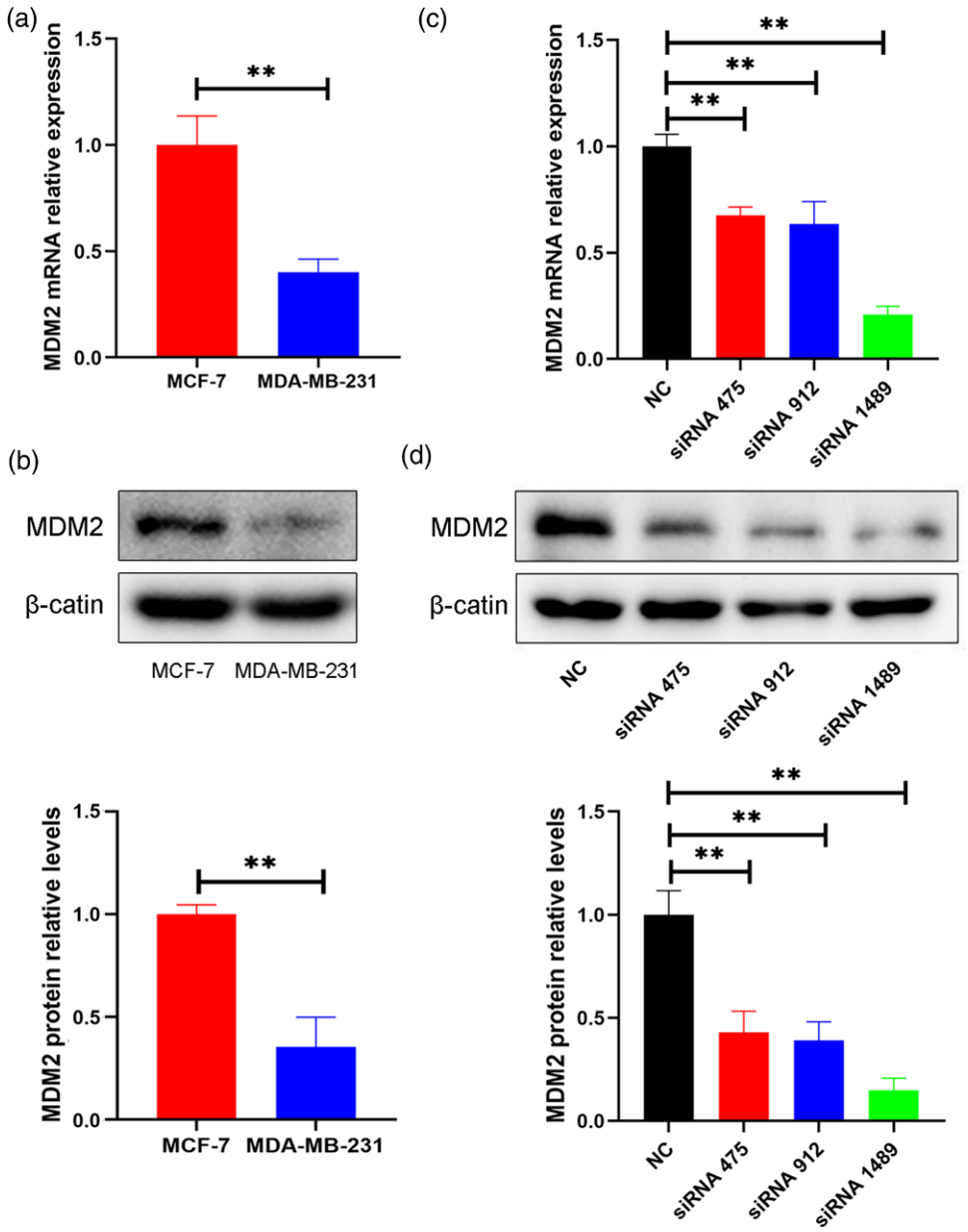


MDM2 expression in breast cancer cell lines and the inhibitory efficiency of siRNA. (a) MDM2 mRNA relative expression ($P = 0.002$). (b) MDM2 protein relative expression ($P = 0.002$). (c) MDM2 mRNA relative expression after transfecting siRNA in MCF-7 cells (NC vs. siRNA 475, $P = 0.0014$; NC vs. siRNA 912, $P = 0.0007$; NC vs. siRNA 1489, $P < 0.0001$). (d) MDM2 protein relative expression after transfecting siRNA in MCF-7 cells (NC vs. siRNA 475, $P = 0.0004$; NC vs. siRNA 912, $P = 0.0002$; NC vs. siRNA 1489, $P < 0.0001$). Data are presented as the mean ± SD based on three independent experiments. $^{*}P < 0.05$; $^{**}P < 0.01$ vs. the NC group. MCF, Michigan Cancer Foundation; $^{99m}$Tc, technetium-99m; MDM2, Murine double minute 2; NC, negative control; siRNA, small interfering RNA.

in MCF-7 and MDA-MB-231 mRNA were 1 ± 0.14 and 0.40 ± 0.06 ($P < 0.05$; $n = 3$), respectively (Fig. 1a). The protein levels in MCF-7 and MDA-MB-231 cells were 1 ± 0.05 and 0.35 ± 0.15 ($P < 0.05$; $n = 3$), respectively (Fig. 1b). This indicated that MCF-7 cells had a high level of MDM2 and were suitable for the imaging experiment.

### Inhibitory effects of small interfering RNA *in vitro*

Three siRNA sequences were designed and their inhibitory effects were investigated to select the best siRNA. The inhibitory effects of each siRNA were estimated according to the protein expression and mRNA content determined by western blots and qRT-PCR (Fig. 1c and d). The results of transfection with the three siRNA sequences showed substantially lower MDM2 mRNA and protein levels than those of the negative control siRNA and blank control groups transfected with Opti-MEM ($P < 0.05$; $n = 3$). There were no significant differences between the three siRNA sequences.

### In-vitro $^{99m}$Tc-HYNIC-siRNA stability

The labeling efficiencies of [$^{99m}$Tc]HYNIC-siRNA 1489 and [$^{99m}$Tc]HYNIC-control siRNA were 62.17 ± 3.16% and 61.56 ± 4.08% ($P > 0.05$; $n = 4$), respectively. The radiochemical purity of the probes was greater than 94% after purification. When the probes were tested at normal temperature (37 °C), the radiochemical purity did not significantly change ($n = 3$). With increasing incubation time, the probes were stable within 6 h and did not show significant degradation. Similarly, there was no difference between cultures in PBS and FBS (Fig. 2a). This indicated that the probes had relatively stable physicochemical properties.

### In-vitro inhibitory effect of siRNA1489 after labeling with technetium-99m

We tested the effect of [$^{99m}$Tc]HYNIC-siRNA 1489 via qRT-PCR and western blots in MCF-7 cell lines. There was an obvious inhibitory effect of siRNA 1489 without $^{99m}$Tc labeling. We compared the results for siRNA 1489 labeled with $^{99m}$Tc to unlabeled siRNA 1489 and blank control. From our experiments, radiolabeling of siRNA 1489 did not alter the effect of RNAi (Fig. 2b and c). [$^{99m}$Tc]HYNIC-siRNA 1489 inhibited the expression of MDM2. The relative expression levels of MDM2 mRNA and protein were 0.34 ± 0.06 and 0.46 ± 0.09 ($P < 0.05$; $n = 3$), respectively (Fig. 2b and c). This indicated that

**Fig. 2**

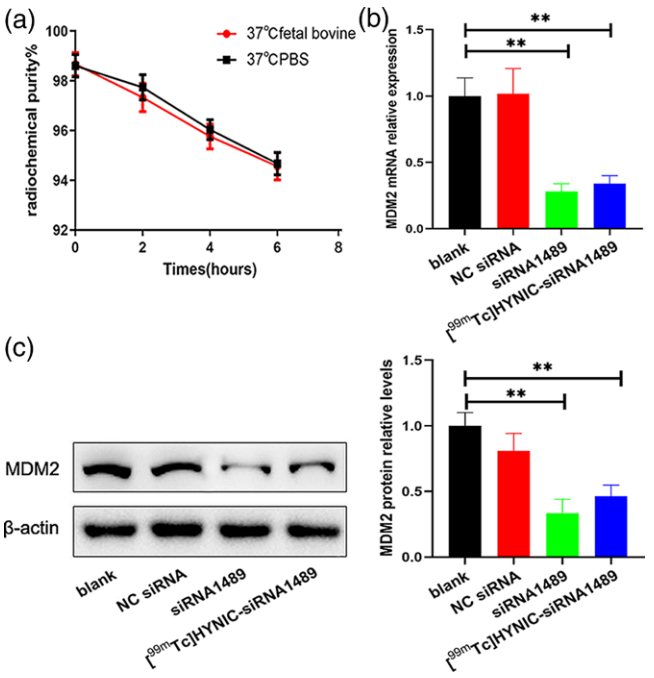


Stability and biological activity of [$^{99m}$Tc]HYNIC-siRNA *in vitro*. (a) Radiochemical purity of [$^{99m}$Tc]HYNIC-siRNA incubated in PBS and bovine serum at 37 °C. (b) MDM2 mRNA relative expression after transfection with NC siRNA, siRNA 1489 and [$^{99m}$Tc]HYNIC-siRNA 1489 measured by qRT-PCR (blank vs. NC siRNA, $P = 0.9970$; blank vs. siRNA 1489, $P < 0.0001$; NC vs. [$^{99m}$Tc]HYNIC-siRNA 1489, $P < 0.0001$). (c) MDM2 protein relative expression after transfection with NC siRNA, siRNA 1489 and [$^{99m}$Tc]HYNIC-siRNA 1489 measured by western blots (blank vs. NC siRNA, $P = 0.2116$; blank vs. siRNA 1489, $P = 0.0003$; NC vs. [$^{99m}$Tc]HYNIC-siRNA 1489, $P = 0.0013$). Data are presented as the mean ± SD based on three independent experiments. $^{*}P < 0.05$; $^{**}P < 0.01$ vs. the blank group. $^{99m}$Tc, technetium-99m; MDM2, Murine double minute 2; NC, negative control; qRT-PCR, quantitative real-time PCR; siRNA, small interfering RNA.

**Fig. 3**

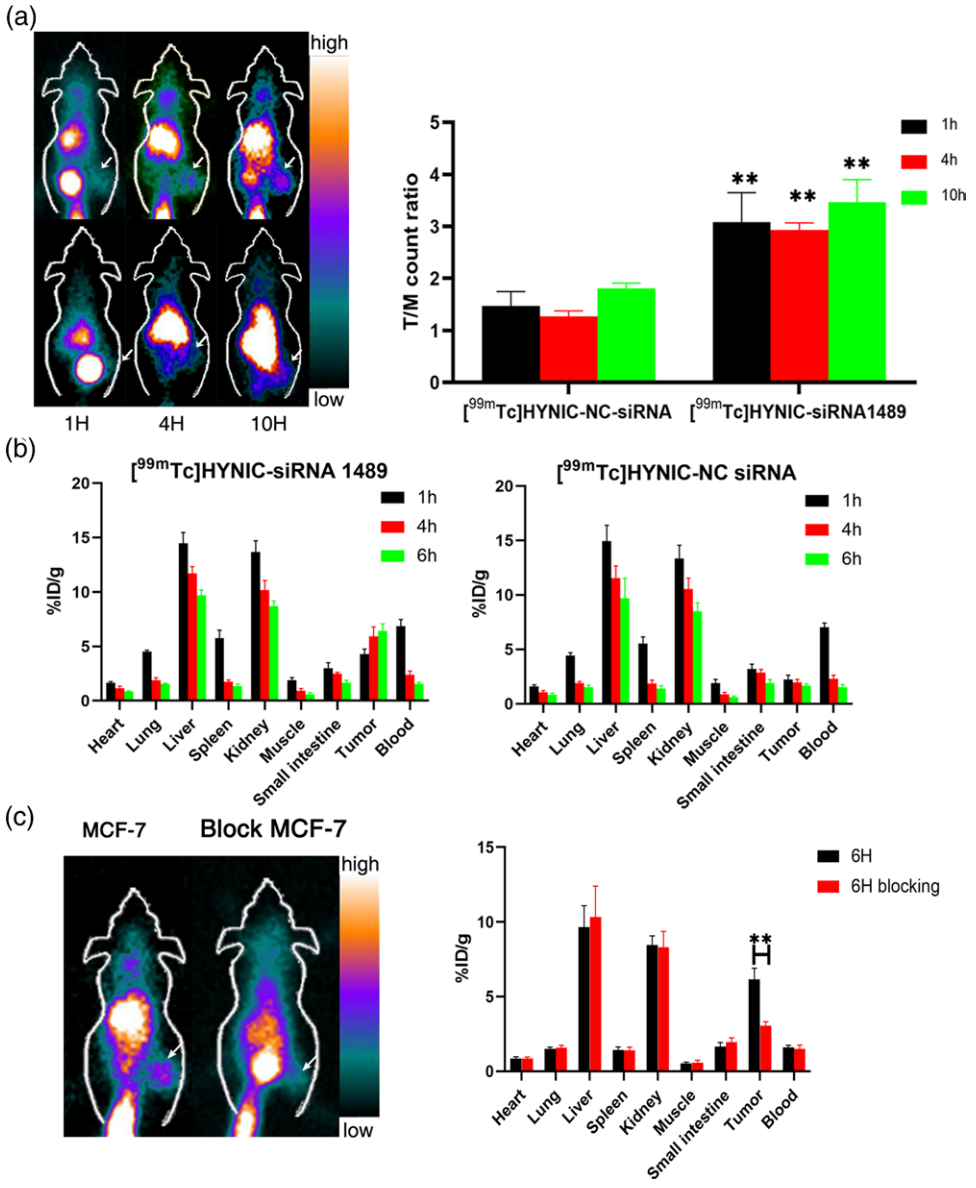


The imaging study of [$^{99m}$Tc]HYNIC-siRNA in NU/NU mice xenografts. (a) The imaging and ratio of tumor to contralateral muscles (T/M) in mice injected with [$^{99m}$Tc]HYNIC-siRNA (upper) and [$^{99m}$Tc]HYNIC-NC siRNA (lower) at different time points (1 h, $P = 0.0115$; 4 h, $P < 0.0001$; 10 h, $P = 0.0029$). (b) The biodistribution of [$^{99m}$Tc]HYNIC-siRNA (upper) and [$^{99m}$Tc]HYNIC-NC siRNA (lower) in mice. (c) SPECT images and biodistribution of MCF-7 and blocked-MCF-7 (6 h vs. 6 h blocking, $P = 0.0025$). Data are presented as mean ± SD based on four independent experiments. $^{*}P < 0.05$, $^{**}P < 0.01$ vs. the NC group. MCF, Michigan Cancer Foundation; $^{99m}$Tc, technetium-99m; siRNA, small interfering RNA; SPECT, single-photon emission computed tomography.

siRNA conjugated with $^{99m}$Tc could be applied to in-vitro experiments.

### Murine double minute 2 molecular imaging

Nude mice with MCF-7 xenografts were used for molecular imaging. The tumors were observed by SPECT at 1, 4, and 10 h after injection of [$^{99m}$Tc]HYNIC-siRNA 1489 or the negative control, [$^{99m}$Tc]HYNIC-NC siRNA. We detected a distinct difference between the [$^{99m}$Tc]HYNIC-siRNA 1489 and [$^{99m}$Tc]HYNIC-NC siRNA groups as the T/M ratios were 3.079 ± 0.57 and 1.472 ± 0.27 ($P < 0.05$; $n = 6$) at 1 h, and were 2.927 ± 0.14 and 1.272 ± 0.11 at 4 h, respectively (Fig. 3a). Furthermore, with increased time, the images of tumors in mice injected with [$^{99m}$Tc]HYNIC-siRNA 1489 were clearer than the negative control group injected with [$^{99m}$Tc]HYNIC-NC siRNA. At 10 h, the T/M ratios reached a peak: [$^{99m}$Tc]HYNIC-siRNA 1489 was 3.465 ± 0.43 and [$^{99m}$Tc]HYNIC-NC siRNA was

1.804 ± 0.11 (Fig. 3a). In the NC group, the imaging of mouse tumors was not observed at every time point. The blocking experiment was used to assess the specificity of [$^{99m}$Tc]HYNIC-siRNA 1489 (Fig. 3c). The accumulation of [$^{99m}$Tc]HYNIC-siRNA 1489 pretreated with siRNA 1489 was lower than that without siRNA 1489 in MCF-7 xenografts. Our results showed that the MDM2 molecular probe could reveal MDM2 transcription levels *in vivo*.

### Biodistribution studies

Following the imaging experiments, we measured the biodistribution of the probes in nude mice using a gamma counter (Fig. 3b). Mice injected with [$^{99m}$Tc]HYNIC-siRNA 1489 showed high accumulation of nuclide in the tumor at 1 and 4 h (4.28 ± 0.47% ID/g and 5.93 ± 0.86% ID/g; $n$ = 6), respectively. The accumulation of [$^{99m}$Tc] HYNIC-siRNA 1489 rose to a peak at 6 h (6.42 ± 0.66% ID/g). Mice injected with [$^{99m}$Tc]HYNIC-NC siRNA did not display an obvious accumulation of nuclide in the tumor at the different time points (2.24 ± 0.39% ID/g, 1.96 ± 0.28% ID/g and 1.66 ± 0.17% ID/g). Based on these data, we thought that [$^{99m}$Tc]HYNIC-siRNA 1489 would be taken up by the tumor and have a long retention time. There was high accumulation in the liver (14.92 ± 1.46% ID/g in the NC group and 14.48 ± 0.99% ID/g in the siRNA 1489 group) and kidney (13.34 ± 1.22% ID/g in the NC group and 13.65 ± 1.05% ID/g in the siRNA 1489 group) in both groups at 1 h. The radioactivity in the liver and kidney decreased over time. This signified that the molecular probe was cleared via the urinary system and the liver.

## Discussion

In recent years, molecular biology technology has developed rapidly. Imaging used for the diagnosis of disease is no longer limited to anatomical imaging. Gene imaging reveals changes in cellular physiological processes at the genetic level, and it has the potential to aid early and accurate diagnosis. In gene imaging, RNAi technology has become a hot research topic as siRNA can effectively combine with target gene mRNA. In the past few decades, the therapeutic potential of siRNA has been confirmed in diseases such as viral infections and cancers [16–18].

The key to molecular imaging is to synthesize molecular probes that target the tumor. It also requires the target tissue to overexpress certain molecules such as proteins or nucleic acids. In this study, *MDM2* was selected as the target gene as it plays an important role in different tumor cells [19–21]. *MDM2* is the major downstream regulator gene of p53. It can form a negative feedback loop with p53, leading to its degradation via ubiquitination and proteasomes. Mutation of *p53* in different cancers will cause immortalization of cells, which is the first step in tumorigenesis [22]. However, the expression of p53 in cancer cells is too low to be detected *in vivo* by noninvasive methods. As a negative regulator, the content of MDM2 could indirectly reflect the content of p53. Park found that different types of breast cancer that express high levels of MDM2 in both the nucleus and cytoplasm were more malignant [23]. Therefore, the early detection of MDM2 is vitally important for the diagnosis and treatment of tumors. In our research, we selected two types of breast cancer cells with different expression levels of MDM2. The PCR results proved that MCF-7 cells expressed MDM2 at higher levels. To select a suitable siRNA, three different siRNAs against MDM2 were designed. The results of PCR and western blots revealed that siRNA 1489 was the best choice; thus, it was used in subsequent experiments.

We used TurboFect as a carrier in the in-vivo experiments, and it is lipophilic and is often used for nonviral transfection. TurboFect can combine with siRNA through electrostatic interactions, and TurboFect-siRNA is adsorbed to the electronegative cytomembrane and transferred into the cells. Then siRNA and DNA could bind and play a role. In general, cells can take in large molecules via endocytosis, and small molecules can enter cells through specific channels or transporters. However, there is no specific channel for siRNA, and it is easily excreted by the reticuloendothelial system. Hence, the targeting efficiency may decrease *in vivo*, so we attempted to increase the probe uptake using TurboFect for in-vivo experiments. In order to solve the problem of rapid degradation and excretion of siRNA *in vivo*, double-strand siRNA was selected in these experiments. As the half-life of double-chain siRNA is longer than that of single-chain siRNA, the inhibitory efficiency of double-chain siRNA is significantly higher than that of single-chain siRNA [24]. Furthermore, we used a *2′*OMe modification for the sense strand of siRNA as this modification did not affect RNA silencing and splicing. This is one of the compatible modification methods, as it not only increased the resistance of siRNA to nucleases but also enhanced the interference effect of siRNA and its thermal stability [14]. In order to enhance the binding of siRNA to the target gene, we added two free double thymine bases on the *3′*-end [15]. The amino modification on the *5′*-end was used to couple with HYNIC. Finally, HYNIC was chelated with $^{99m}TcO_4^-$. At the same time, the coligands, tricine and EDDA, were added to occupy the void position of $^{99m}TcO_4^-$. The PCR and western blot results showed that [$^{99m}$Tc]HYNIC-siRNA 1489 significantly inhibited the expression of MDM2 mRNA and protein after transfection of MCF-7 cells. In addition to the characteristics of the molecular probe, radiochemical purity and labeling efficiency were also important. If the radiochemical purity of the probe was low, excessive free $^{99m}TcO_4^-$ will be absorbed by the thyroid, which would interfere with tumor imaging. Similarly, if the labeling efficiency was low, the molecular probe injected into the nude mice would be taken up at lower levels. All of these factors will affect the imaging. Therefore, we

used chromatography to determine the radiochemical purity and labeling efficiency after purifying the molecular probe, and the results were satisfactory. The stability of the siRNA-MDM2 probe was validated in PBS and serum, which provided a basis for imaging animal tumors.

In these experiments, the [$^{99m}$Tc]HYNIC-siRNA 1489 inhibition rate of MDM2 mRNA *in vitro* reached approximately 70%. The western blot results showed that the inhibition of MDM2 protein was also substantial. To detect the specificity of the probe, [$^{99m}$Tc]HYNIC-siRNA 1489 and [$^{99m}$Tc]HYNIC-control siRNA were injected into mice in the in-vivo experiments. Tumor images of the control group injected with [$^{99m}$Tc]HYNIC-control siRNA were not detected by SPECT. Furthermore, the tumors in the probe group injected with [$^{99m}$Tc]HYNIC-siRNA 1489 were clearly delineated. The T/M ratios of the tumors in the molecular probe group were higher than those in the control group. With time, the images of the tumors became clearer. This indicated that the probe had sufficient retention time in the tumor, and siRNA could bind to the target genes specifically and be available for gene targeted imaging.

### Conclusion

In this article, we synthesized an imaging probe targeting MDM2 in breast cancer. Our results demonstrated that [$^{99m}$Tc]HYNIC-siRNA accumulated in the tumors and had a sufficiently long retention time to allow imaging. SPECT imaging also indirectly reflected MDM2 expression levels. In summary, [$^{99m}$Tc]HYNIC-siRNA SPECT imaging might be an effective method for assessing MDM2 expression via in-vivo imaging.

## Acknowledgements

This study was supported by the National Natural Science Foundation of China (grant numbers: 81671714 and 81771864). The funders had a role in the design of the research, and writing the manuscript.

Data availability statement: the full data used and analyzed during the current study are available on reasonable request from the corresponding authors.

Posted history: this manuscript was previously posted to https://doi.org/10.21203/rs.3.rs-49584/v1.

### Conflicts of interest

There are no conflicts of interest.

## References

1 DeSantis CE, Ma J, Gaudet MM, Newman LA, Miller KD, Goding Sauer A, *et al*. Breast cancer statistics, 2019. *CA Cancer J Clin* 2019; **69**:438–451.
2 Shvarts A, Steegenga WT, Riteco N, van Laar T, Dekker P, Bazuine M, *et al*. MDMX: a novel p53-binding protein with some functional properties of MDM2. *EMBO J* 1996; **15**:5349–5357.
3 Kubbutat MH, Jones SN, Vousden KH. Regulation of p53 stability by Mdm2. *Nature* 1997; **387**:299–303.
4 Haupt Y, Maya R, Kazaz A, Oren M. Mdm2 promotes the rapid degradation of p53. *Nature* 1997; **387**:296–299.
5 Honda R, Tanaka H, Yasuda H. Oncoprotein MDM2 is a ubiquitin ligase E3 for tumor suppressor p53. *FEBS Lett* 1997; **420**:25–27.
6 Fan Y, Ma K, Jing J, Wang C, Hu Y, Shi Y, *et al*. Recombinant dual-target MDM2/MDMX inhibitor reverses doxorubicin resistance through activation of the TAB1/TAK1/p38 MAPK pathway in wild-type p53 multidrug-resistant breast cancer cells. *J Cancer* 2020; **11**:25–40.
7 Feng FY, Zhang Y, Kothari V, Evans JR, Jackson WC, Chen W, *et al*. MDM2 inhibition sensitizes prostate cancer cells to androgen ablation and radiotherapy in a p53-dependent manner. *Neoplasia* 2016; **18**:213–222.
8 Tong H, Zhao K, Zhang J, Zhu J, Xiao J. YB-1 modulates the drug resistance of glioma cells by activation of MDM2/p53 pathway. *Drug Des Devel Ther* 2019; **13**:317–326.
9 Liu Y, Xing ZB, Wang SQ, Chen S, Liu YK, Li YH, *et al*. MDM2-MOF-H4K16ac axis contributes to tumorigenesis induced by Notch. *FEBS J* 2014; **281**:3315–3324.
10 Thirumurthi U, Shen J, Xia W, LaBaff AM, Wei Y, Li CW, *et al*. MDM2-mediated degradation of SIRT6 phosphorylated by AKT1 promotes tumorigenesis and trastuzumab resistance in breast cancer. *Sci Signal* 2014; **7**:ra71.
11 Fan Y, Li M, Ma K, Hu Y, Jing J, Shi Y, *et al*. Dual-target MDM2/MDMX inhibitor increases the sensitization of doxorubicin and inhibits migration and invasion abilities of triple-negative breast cancer cells through activation of TAB1/TAK1/p38 MAPK pathway. *Cancer Biol Ther* 2019; **20**:617–632.
12 Lu J, McEachern D, Li S, Ellis MJ, Wang S. Reactivation of p53 by MDM2 inhibitor MI-77301 for the treatment of endocrine-resistant breast cancer. *Mol Cancer Ther* 2016; **15**:2887–2893.
13 Ku SH, Jo SD, Lee YK, Kim K, Kim SH. Chemical and structural modifications of RNAi therapeutics. *Adv Drug Deliv Rev* 2016; **104**:16–28.
14 Chiu YL, Rana TM. siRNA function in RNAi: a chemical modification analysis. *RNA* 2003; **9**:1034–1048.
15 Choung S, Kim YJ, Kim S, Park HO, Choi YC. Chemical modification of siRNAs to improve serum stability without loss of efficacy. *Biochem Biophys Res Commun* 2006; **342**:919–927.
16 Müller K, Klein PM, Heissig P, Roidl A, Wagner E. EGF receptor targeted lipo-oligocation polyplexes for antitumoral siRNA and miRNA delivery. *Nanotechnology* 2016; **27**:464001.
17 Zhang M, Wang X, Han MK, Collins JF, Merlin D. Oral administration of ginger-derived nanolipids loaded with siRNA as a novel approach for efficient siRNA drug delivery to treat ulcerative colitis. *Nanomedicine (Lond)* 2017; **12**:1927–1943.
18 Jose A, Labala S, Venuganti VV. Co-delivery of curcumin and STAT3 siRNA using deformable cationic liposomes to treat skin cancer. *J Drug Target* 2017; **25**:330–341.
19 Li W, Wang SS, Deng J, Tang JX. Association of p73 gene G4C14-A4T14 polymorphism and MDM2 gene SNP309 with non-small cell lung cancer risk in a Chinese population. *Oncol Lett* 2017; **14**:1817–1822.
20 Davoodi P, Srinivasan MP, Wang CH. Effective co-delivery of nutlin-3a and p53 genes via core-shell microparticles for disruption of MDM2-p53 interaction and reactivation of p53 in hepatocellular carcinoma. *J Mater Chem B* 2017; **5**:5816–5834.
21 Chaudhary R, Muys BR, Grammatikakis I, De S, Abdelmohsen K, Li XL, *et al*. A circular RNA from the MDM2 locus controls cell cycle progression by suppressing p53 levels. *Mol Cell Biol* 2020; **40**:e00473–e00419.
22 Kaul SC, Aida S, Yaguchi T, Kaur K, Wadhwa R. Activation of wild type p53 function by its mortalin-binding, cytoplasmically localizing carboxyl terminus peptides. *J Biol Chem* 2005; **280**:39373–39379.
23 Park HS, Park JM, Park S, Cho J, Kim SI, Park BW. Subcellular localization of Mdm2 expression and prognosis of breast cancer. *Int J Clin Oncol* 2014; **19**:842–851.
24 Liao H, Wang JH. Biomembrane-permeable and Ribonuclease-resistant siRNA with enhanced activity. *Oligonucleotides* 2005; **15**:196–205.